Medicinal Chemistry Research
https://doi.org/10.1007/s00044-021-02782-x

MEDICINAL CHEMISTRY RESEARCH

ORIGINAL RESEARCH

The potential of 4-aryl-6-morpholino-3(2*H*)-pyridazinone-2-arylpiperazinylacetamide as a new scaffold for SIRT2 inhibition: in silico approach guided by pharmacophore mapping and molecular docking

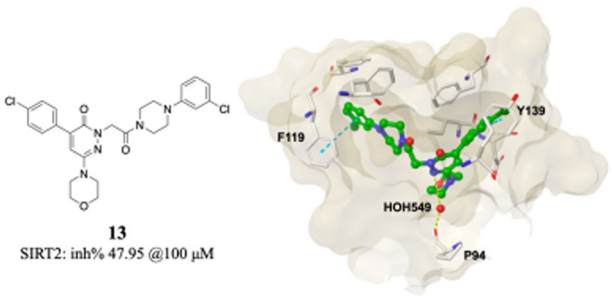
Murat Kadir Sukuroglu[1] · Mahmut Gozelle[1] · Yesim Ozkan[2] · Gokcen Eren[1]

Received: 24 June 2021 / Accepted: 9 August 2021
© The Author(s), under exclusive licence to Springer Science+Business Media, LLC, part of Springer Nature 2021

Abstract

Numerous studies have demonstrated that the aberrant enzymatic activity of SIRTs has been linked to various diseases like diabetes, cancer, inflammation, cardiovascular diseases, neurodegenerative disorders and therefore, the modulation of SIRTs is of therapeutic importance. The pharmacological action of substituted pyridazinones has been broadly studied and has received much attention on account of especially their cardiovascular, anticancer, anti-inflammatory, and analgesic activity. From this point of view, we evaluated our in-house compounds bearing substituted pyridazinone skeleton for their in vitro inhibitory potency against SIRT2 and the results were supported both by the compatibility with the pharmacophore model previously developed for selective SIRT2 inhibitors and by the interaction fingerprints in hSIRT2 active site. The results revealed that 4-aryl-6-morpholino-3(2*H*)-pyridazinone functionalized amide scaffold showing 48% inhibition against SIRT2 may be considered as a starting point in the development of new type SIRT2 inhibitors.

Graphical Abstract



Keywords SIRT2 · Pyridazinone · Pharmacophore mapping · Molecular Docking

Introduction

Sirtuins (SIRTs) are a conserved family of proteins found in a wide range of organisms from bacteria to mammals acting as substrate-specific type III protein lysine deacetylases. Although the first enzymatic activity of SIRTs was the NAD^+-dependent deacetylation of both histone and nonhistone proteins, recent studies have shown that SIRTs catalyze a growing list of more general deacylation reactions including ADP-ribosylation [1], demyristoylation [2], and desuccinylation [3]. Mammals have seven

These authors contributed equally: Murat Kadir Sukuroglu, Mahmut Gozelle

✉ Murat Kadir Sukuroglu
mkadir@gazi.edu.tr

[1] Department of Pharmaceutical Chemistry, Faculty of Pharmacy, Gazi University, 06330 Ankara, Turkey

[2] Department of Biochemistry, Faculty of Pharmacy, Gazi University, 06330 Ankara, Turkey

Published online: 25 August 2021

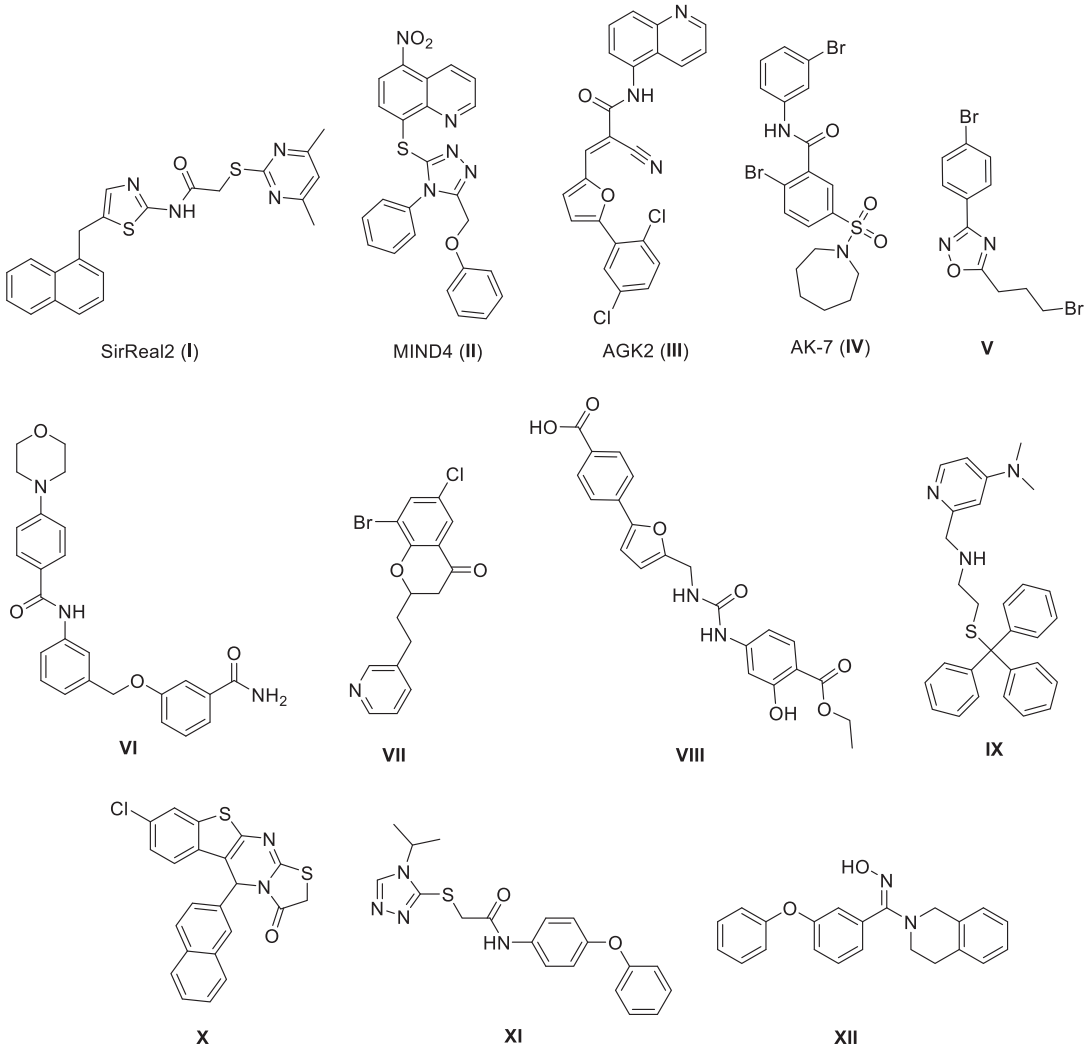
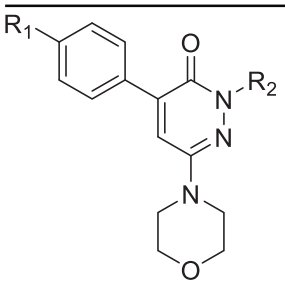


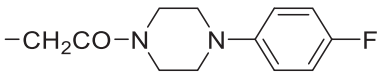
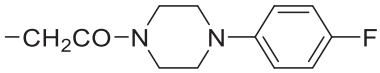
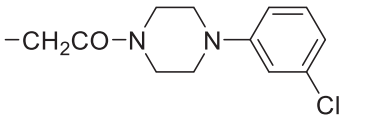
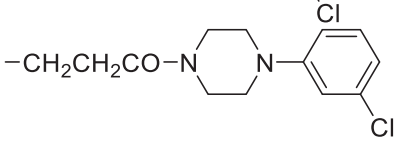
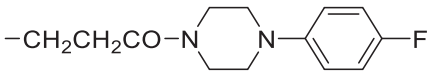
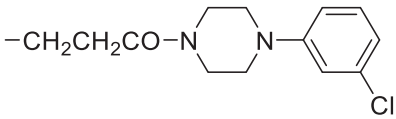
Fig. 1 Chemical structures of known SIRT2 inhibitors

sirtuin isoforms (SIRT1-7) with various subcellular localizations and functions [4, 5]. Of interest, SIRT2 is the only SIRT family member which is mainly a cytoplasmic protein but it is transported to the nucleus during mitosis [6]. Many new substrates and proteins associated to SIRT2 have been identified during last decade, such as FOXO1/3a, PGAM2, CDK9, Par-3, G6PD, p53, and α-tubulin [7–11]. In modulating various biological processes, SIRT2 plays different function, such as energy metabolism, cell cycle regulation, autophagy, DNA repair, and pathological processes, including tumors and neurodegenerations [5, 12–15]. Although SIRT2 has been recognized as tumor suppressor, recent studies showed that overexpression of SIRT2 is mainly related to cancer and neurodegenerative diseases [6, 16]. Besides, numerous studies showed that the significant anticancer effect of SIRT2 inhibitors due to the overexpression of SIRT2 in various cancers such as breast cancer, cervical cancer and leukemia [17–19]. Interestingly, it seems that both inhibition and activation of SIRT2 may have therapeutic potential. As a result, the complicated activity of SIRT2 requires further studies and development of vehicle molecules to support these efforts.

A number of SIRT2 inhibitors have been discovered so far with different chemical structure, including SirReal2 (**I**) [20], MIND4 (**II**) [21], AGK2 (**III**) [22], AK-7 (**IV**) [23], 1,2,4-oxadiazole derivatives (**V**) [19], nicotinamide derivatives (**VI**) [24], 4-chromanone derivatives (**VII**) [25], (5-phenylfuran-2-yl)methanamine derivatives (**VIII**) [26], S-trityl-L-cysteine derivatives (**IX**) [27], benzothieno[3,2-d] pyrimidine derivatives (**X**) [28], *N*-(aryloxyaryl)acetamide derivatives (**XI**) [29], and aryloxybenzamide derivatives (**XII**) [30] (Fig. 1). Although, there have been many attempts to discover the therapeutic potential of SIRT2 with small-molecule inhibitors, there is still no drug that approved for clinical use. Hence, new SIRT2 inhibitors

Table 1 Chemical structures of in-house pyridazinone derivatives



Comp	R_1	R_2	Comp.	R_1	R_2
1	–H	$-CH_2COOH$	**9**	–Cl	$-CH_2CH_2COOH$
2	–H	$-CH_2COOH_2CH_3$	**10**	–Cl	$-CH_2CH_2COOH_2CH_3$
3	–H	$-CH_2CH_2CN$	**11**	–H	
4	–H	$-CH_2CH_2COOH$	**12**	–Cl	
5	–H	$-CH_2CH_2COOCH_2CH_3$	**13**	–Cl	
6	–Cl	$-CH_2COOH$	**14**	–H	
7	–Cl	$-CH_2COOH_2CH_3$	**15**	–Cl	
8	–Cl	$-CH_2CH_2CN$	**16**	–Cl	

which have better bioavailability, lower toxic side effects with improved potency and selectivity are still needed.

Pyridazinone, the six membered nitrogen containing ring has aroused a great deal of attention due to its wide spectrum of biological activities and therapeutic applications. Therefore, many pyridazinone-based compounds targeting different diseases have been reported by researchers highlighting its status in the development of novel drug candidates [31]. A survey of literature revealed that substituted pyridazinones possessed analgesic and anti-inflammatory activities [32–36], where many of them exhibited antiproliferative activity against various cancer cell lines [37–40]. In addition, a number of neuroprotective compounds with pyridazinone moiety were reported [41–43]. Since the reported activities of pyridazinone-based compounds overlap with the diseases in which the SIRT2 enzyme is targeted, the presence of SIRT2 inhibitory effects was expected in our in-house compounds including pyridazinone derivative which were reported previously [32] for their potent analgesic activity (Table 1). Therefore, we evaluated these compounds for their in vitro SIRT2 inhibitory potency. The results were examined by comparing the interaction patterns obtained with key residues in SIRT2 active site and the compatibility of docked conformations to the pharmacophore model previously generated for selective SIRT2 inhibitors [29].

Results and discussion

The in-house compounds including sixteen substituted pyridazinone derivatives reported previously [32] were screened for their SIRT2 inhibitory potency with in vitro assay using recombinant SIRT2 enzyme at 100 µM concentration, while suramin was used as reference compound.

As presented in Table 2, among the compounds tested, SIRT2 inhibitory activity was observed for only compounds **11–14** which were the amide derivatives of 4-aryl-6-morpholino-3(2*H*)-pyridazinone. The compounds **1–10** bearing propionitrile, acetic acid, propionic acid and corresponding ethyl esters showed no effect on the level of SIRT2 activity. Moreover, no inhibition was detected for the compounds **15** and **16** having arylpiperazinylalkyl chain at the 2-position of pyridazinone ring.

According to results, the presence of a side chain at the 2-position of pyridazinone ring was associated with a moderate level of SIRT2 inhibition which was also supported by molecular docking studies. However, the elongation of the alkyl spacer which linked the amide moiety to the 2-position of pyridazinone, resulted in reduced SIRT2 inhibition. Among the propanamide derivatives (**14**–**16**), only 2-[3-[4-(3-chlorophenyl)piperazin-1-yl]-3-oxopropyl]-6-(morpholin-4-yl)-4-phenyl-3(2*H*)-pyridazinone (**14**) showed inhibitory effect on SIRT2, even if it was slightly poor. Compound **16** was found to be inactive against SIRT2 while the corresponding acetamide analogue (**13**) exhibited significant SIRT2 inhibition. In addition, bearing an unsubstituted or *p*-chloro substituted phenyl ring at the 4-position of pyridazinone had no significant effect on SIRT2 inhibition.

In order to understand the influence of chemical diversity on the enzyme binding and thus on the inhibitory activity, binding patterns of all compounds tested in the active site of hSIRT2 were investigated *via* molecular docking simulations. Moreover, the compatibility of docked conformations to the pharmacophore model previously generated for selective SIRT2 inhibitors was also analyzed. The docking results were found to be well correlated with bioactivity results indicating the importance of key interactions reported for improved SIRT2 inhibition [29, 30, 44]. As shown in Fig. 2, SirReal analogue x-ray coligand interacted the selectivity pocket *via* π–π contacts between its 4,6-dimethylpyrimidine moiety and the pocket residues Y139 and F190. The compound was stabilized by π-π contacts between naphtyl ring and the residues adjacent to substrate binding channel (F119, F131, and F234). In addition, a H-bond was formed between Pro94 and its carbonyl oxygen through the structural water HOH549. The superimposition of bioactive conformation of x-ray coligand with the pharmacophore model [29] comprises of one hydrogen bond acceptor (A) and three aromatic rings (R) was given in Fig. 2B.

Table 2 Inhibitory activities of compounds against SIRT2

Compound	SIRT2 inhibition% (@100 μM)
11	30.80 ± 3.28
12	14.60 ± 1.57
13	47.95 ± 3.59
14	27.84 ± 1.98
Suramin	97.37 ± 0.25

As depicted in Fig. 3, the compounds bearing 4-aryl-6-morpholino-3(2*H*)-pyridazinone scaffold with acetic acid or propionic acid side chain at the 2-position (**1**, **4**, **6**, **9**) and their corresponding ethyl ester analogues (**2**, **5**, **7**, **10**) were found to share similar binding patterns in SIRT2 active site. The morpholine moiety was directed through the selectivity pocket comprising the residues Y139, I169, D170, and F190. The pyridazinone core was anchored in the center of the binding site while the phenyl ring was oriented towards the substrate binding site. The carbonyl oxygen of pyridazinone ring in all compounds interacted with the structural water HOH549 *via* H-bonding which was reported as crucial for SIRT2 inhibition. All compounds except the ester derivatives **2** and **5**, formed H-bond with I169 through carbonyl oxygen of carboxylic acid moiety. No interaction

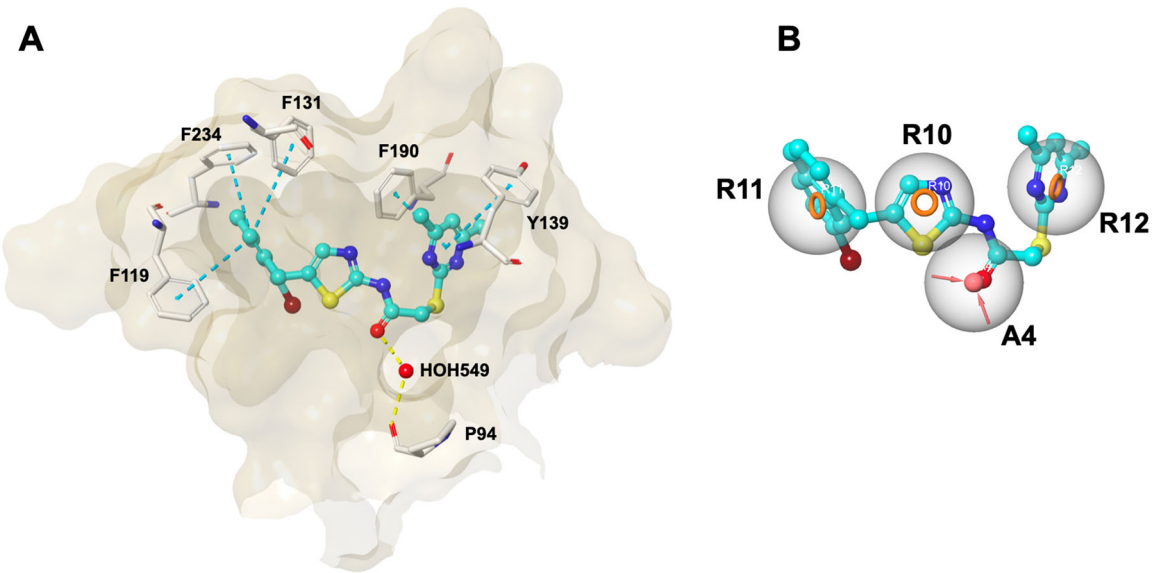


Fig. 2 **A** Binding pattern of x-ray coligand in the active site of SIRT2 (PDB: 5DY4). **B** The superimposition of the bioactive conformation of x-ray coligand with the four featured pharmacophore model (the hollow rings R10, R11, and R12 are aromatic and sphere with vectors A4 is H-bond acceptor feature)

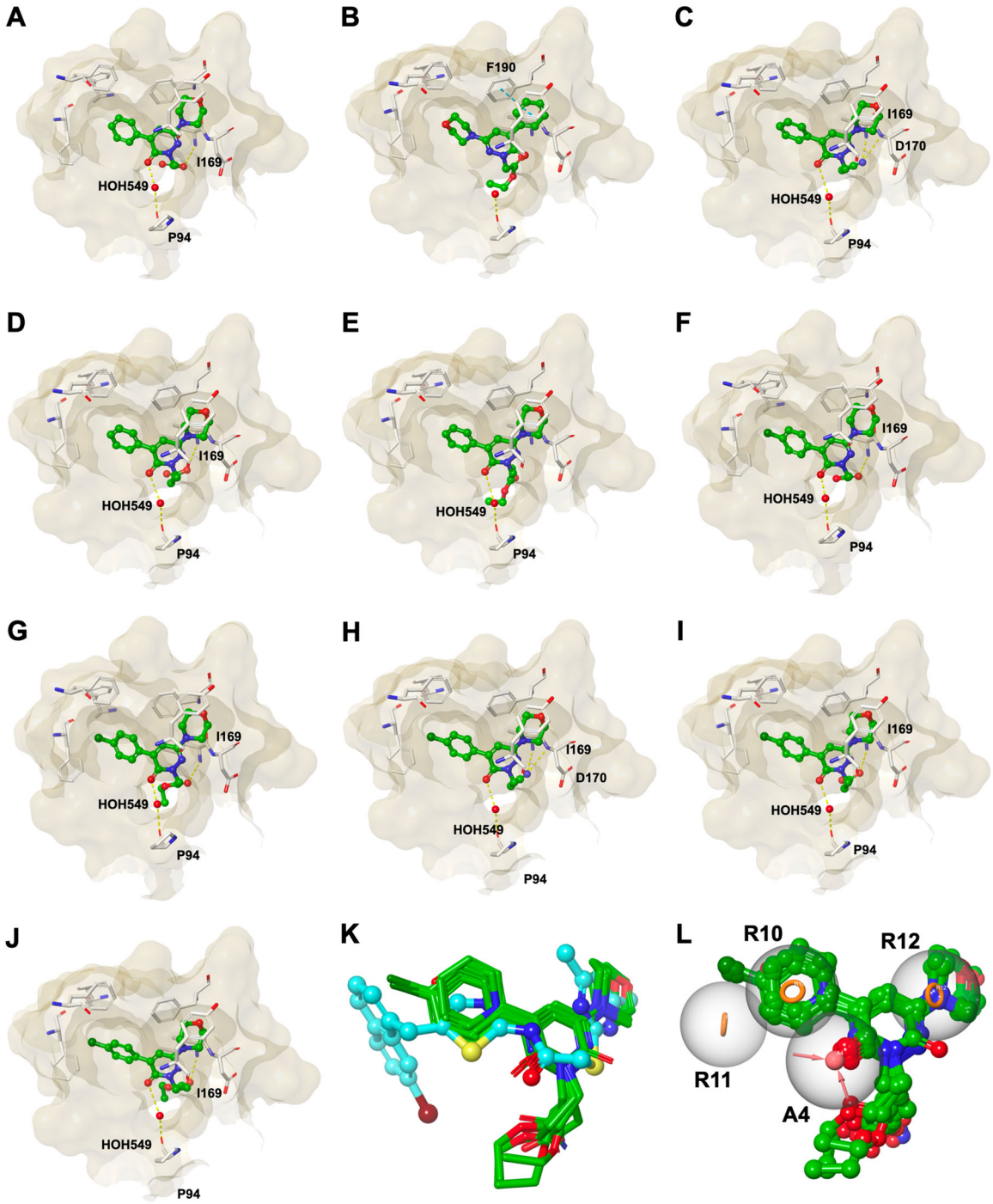


Fig. 3 Binding patterns of the compounds **1** (**A**); **2** (**B**); **3** (**C**); **4** (**D**); **5** (**E**); **6** (**F**); **7** (**G**); **8** (**H**); **9** (**I**); **10** (**J**) in the active site of SIRT2 (PDB: 5DY4). **K** The superimposition of the docked compounds **1–10** (green sticks) with the x-ray coligand (cyan ball and stick). **L** The superimposition of the docked compounds **1–10** (green ball and sticks) with the four featured pharmacophore model (the hollow rings R10, R11, and R12 are aromatic and sphere with vectors A4 is H-bond acceptor feature)

with active site residues was observed for the phenyl moiety at the 4-position of pyridazinone ring.

For the propionitrile derivatives (**3** and **8**), the same binding conformation was observed with those of bearing acetic acid or propionic acid side chain or their corresponding ester derivatives. Due to nitrile group, an additional interaction was observed with D170 in selectivity pocket.

The superimposition of x-ray coligand having selective SIRT2 inhibition potency at nanomolar level [44] and the docked compounds (**1–10**) indicated that those had a missing part in scaffold corresponding to the naphthalene

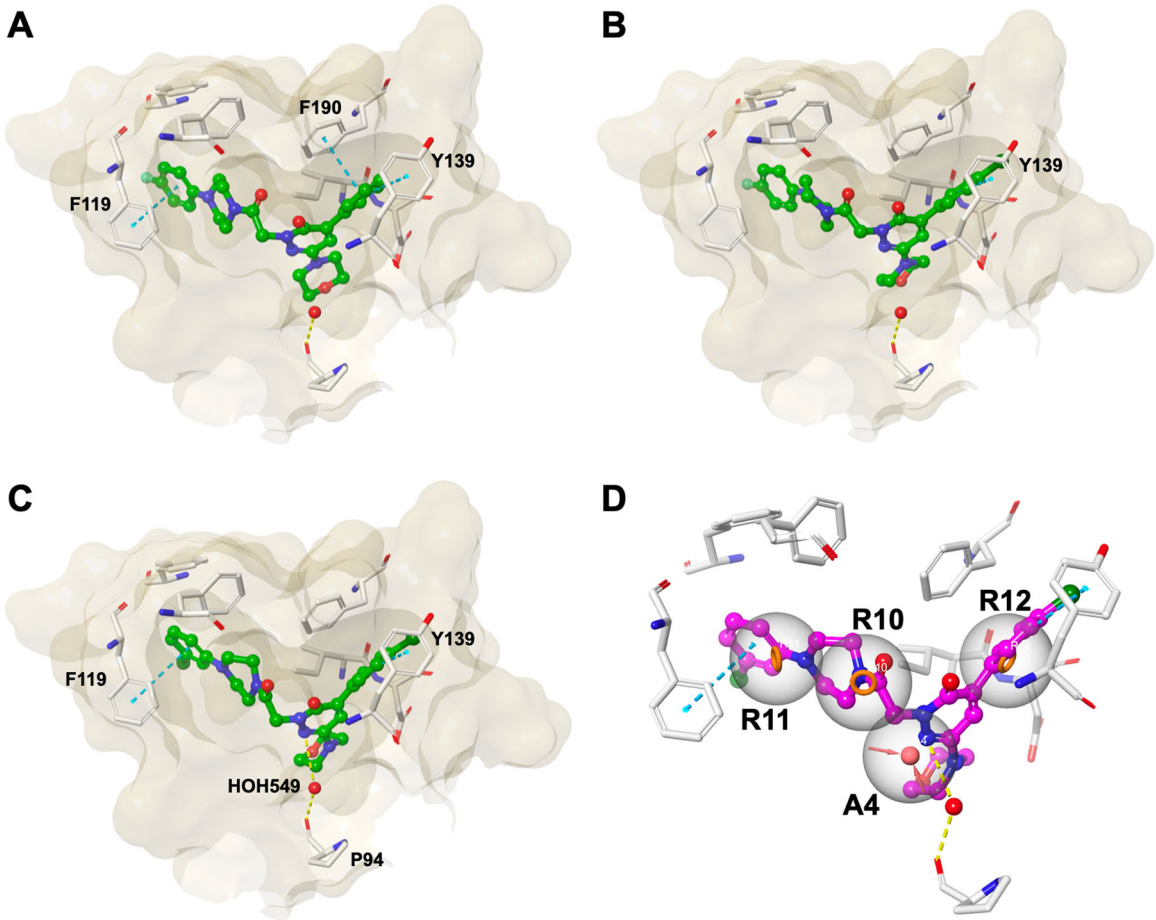


Fig. 4 Binding patterns of the compounds **11** (**A**); **12** (**B**); **13** (**C**) in the active site of SIRT2 (PDB: 5DY4). **D** The superimposition of the docked compound **13** (magenda ball and sticks) with the four featured pharmacophore model (the hollow rings R10, R11, and R12 are aromatic and sphere with vectors A4 is H-bond acceptor feature)

ring which was responsible to form π-π contacts with the aromatic residues of the active site entrance. Although the compounds were able to form interactions with structural water and some of the residues comprising selectivity pocket, the lack of interactions with the entrance may be suggested as an explanation for their inactive profile against SIRT2 (Fig. 3K). This assumption was also highlighted by the examination the compatibility of docked conformations with pharmacophore model indicating the missing part for the feature so called R11 in Fig. 3L.

Among all compounds, those bearing an arylpiperazinyloxoalkyl at the 2-position of pyridazinone ring created a better fit into the active site compared to those of compounds **1**–**10** due to the introduction of bulky side chain on the skeleton (Figs. 4, 5). By the elongation of the side chain at the 2-position, the binding conformations were switched compared to those of compounds **1**–**10**, resulting replacement of morpholine moiety to aryl group at the 4-position of pyridazinone ring which the occupied the selectivity pocket. In case of compounds **11**, **13**, and **16**, the π-π contacts were provided with selectivity pocket residues Y139 and/or F190 by this switch in binding orientation. For compounds **11** and **13**, the terminal phenyl ring of the side chain at the 2-position of pyridazinone, interacted with F119 at the entrance of the binding groove *via* π–π contact.

In the series of compounds having arylpiperazinyloxoethyl side chain (**11**–**13**), H-bonding was observed with the structural water HOH549 through pyridazinone nitrogen for only compound **13**. The superimposition of the docked conformation of **13** revealed that the structure served the best fitting with the pharmacophore model features providing the crucial interactions for SIRT2 inhibition which was well correlated with the bioactivity data. Thus, among all compounds tested, compound **13** exhibited the best inhibition profile against SIRT2, as expected.

Elongation of the alkyl spacer in acetic acid derivatives resulted in loss of SIRT2 inhibition. The compounds bearing arylpiperazinyloxopropyl side chain (**14**–**16**) adopted a bent conformation in active site leading the lack of pharmacophore model fit, thus, lack of interaction with key residues. Although π–π contacts with Y139, F190 for compounds **14** and **16**; H-bonding with structural water

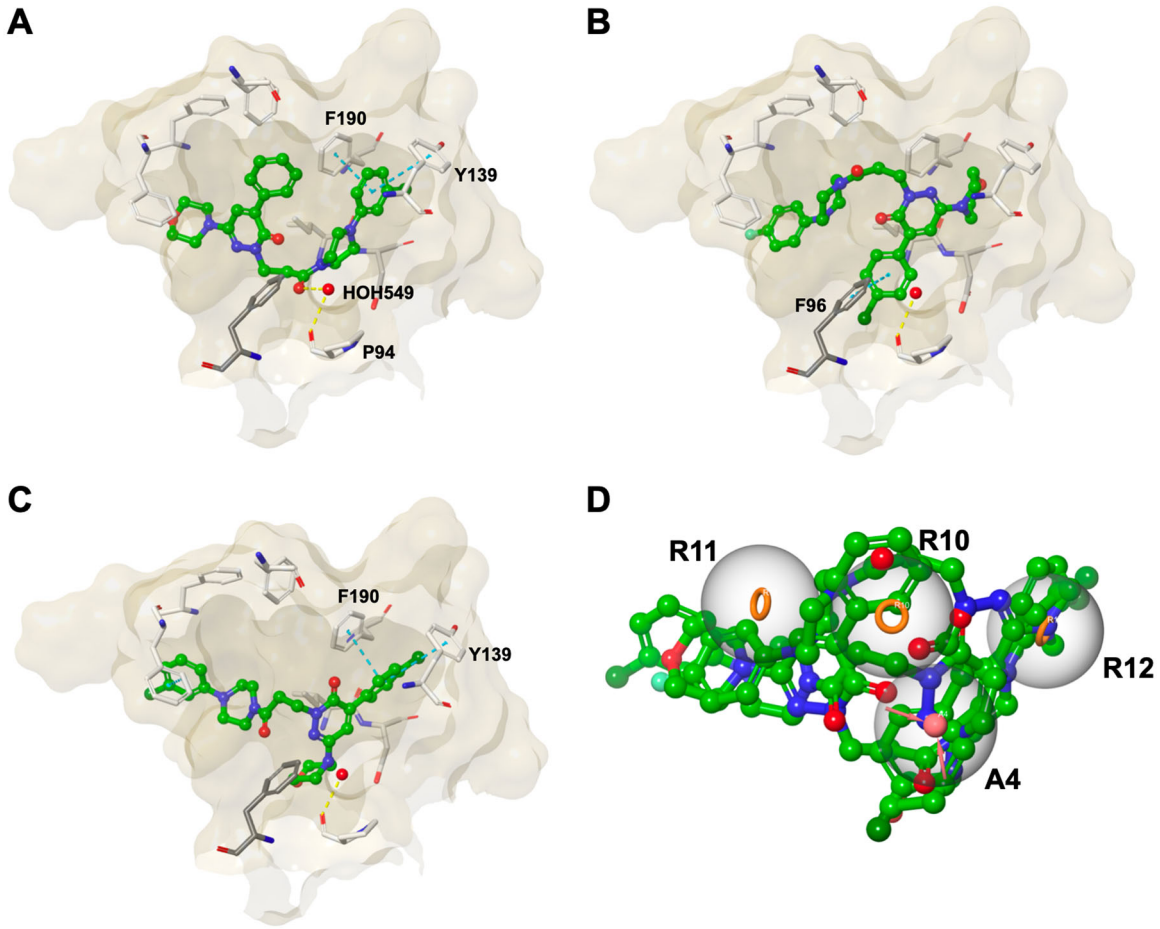


Fig. 5 Binding patterns of the compounds **14** (**A**); **15** (**B**); **16** (**C**) in the active site of SIRT2 (PDB: 5DY4). **D** The superimposition of the docked compounds **14–16** (green ball and sticks) with the four featured pharmacophore model (the hollow rings R10, R11, and R12 are aromatic and sphere with vectors A4 is H-bond acceptor feature)

HOH549 for compound **14**; π–π contact with F96 for compound **15** were observed, they did not seem to contribute enough to an enhanced enzyme–ligand stabilization. The effect of elongation of the alkyl spacer at the 2-position of pyridazinone ring on the binding conformation was represented in Fig. 5D, indicating the oxoethyl spacer provided a better fit for pharmacophore model than oxopropyl spacer. These findings may explain the observed difference in the bioactivity profile for compounds **11–13** and **14–16**, although both series were amide derivatives.

The predicted physically significant descriptors and pharmaceutically relevant properties of the compounds **1–16** calculated by QikProp module (Schrödinger Release 2020-2: QikProp, Schrödinger, LLC, New York, NY, 2020) were listed in Table 3 with the range of values that cause a compound to be flagged as dissimilar to other known drugs. The calculated properties representing druglikeness were found to be within the optimal range for compounds **11–14** which displayed an inhibitory effect against SIRT2. In silico ADMET predictions revealed that except having hERG inhibition potential, the compounds **11–14** showed good predicted blood–brain, Caco, and MDCK permeability. Predicted oral absorption values were found to be high where the human serum albumin binding capacities were calculated within suitable limits [45, 46].

Conclusion

To identify small-molecule inhibitors with new chemical scaffolds targeting SIRT2, an in-house collection including 4-aryl-6-morpholino-3(2*H*)-pyridazinone acid, ester and amide derivatives linked to the position 2 by an alkyl spacer were evaluated for their SIRT2 inhibitory potency. Binding behaviors of tested compounds were also analyzed by molecular docking simulations. The docking results in conjunction with the bioactivity data illustrated the importance of key interaction in SIRT2 active site and the compatibility of docked conformations to the pharmacophore model previously generated for selective SIRT2 inhibition was found to be in a good agreement with the inhibition profile of the compounds. Consequently, 4-aryl-6-

Table 3 Calculated druglikeness and ADMET properties of compounds **1–16**

Cmpd	Druglikeness						ADMET properties							
	#rot	MW	HBD	HBA	Ruleof5	Ruleof3	CNS	LogP	LogHERG	PCaco	LogBB	PMDCK	LogKhsa	HOA%
1	3	315.33	1	6.2	0	0	−1	2.80	−3.25	159.25	−0.79	86.37	−0.17	82.74
2	4	343.38	0	6.2	0	0	0	3.27	−5.30	2061.61	−0.38	1081.36	0.02	100
3	4	310.36	0	5.7	0	0	0	2.78	−4.95	1743.77	−0.40	902.34	−0.16	100
4	4	329.36	1	6.2	0	0	−1	3.13	−3.16	235.86	−0.68	132.04	−0.13	87.72
5	5	357.41	0	6.2	0	0	0	3.49	−5.18	2444.19	−0.35	1299.81	0.05	100
6	3	349.77	1	6.2	0	0	−1	3.28	−3.19	159.34	−0.65	212.99	−0.06	85.59
7	4	377.83	0	6.2	0	0	0	3.79	−5.23	2061.79	−0.22	2665.48	0.15	100
8	4	344.80	0	5.7	0	0	0	3.29	−4.90	1744.73	−0.25	2225.32	−0.03	100
9	4	363.80	1	6.2	0	0	−1	3.62	−3.11	235.89	−0.53	325.49	−0.02	90.59
10	5	391.85	0	6.2	0	0	0	3.99	−5.11	2445.12	−0.19	3204.93	0.17	100
11	3	477.54	0	8.2	0	1	−1	4.32	−5.42	1906.34	−0.18	2477.59	0.19	100
12	3	511.98	0	8.2	1	1	−1	4.83	−5.32	1907.39	−0.02	6110.16	0.32	100
13	3	528.44	0	8.2	2	1	0	5.07	−5.33	1906.94	0.06	8761.73	0.39	89.44
14	4	508.02	0	8.2	1	1	−1	4.85	−5.35	2004.21	−0.15	3563.29	0.34	100
15	4	526.01	0	8.2	1	1	−1	4.67	−4.40	1843.33	−0.01	5970.65	0.23	100
16	4	542.46	0	8.2	2	1	0	5.35	−5.25	2005.32	0.01	8787.67	0.47	91.47

Description of property or descriptors (range or recommended values) were; *#rot* Number of rotatable bonds (0–15), *MW* molecular weight (130.0–725.0), *HBD* estimated number of hydrogen bonds that would be donated by the solute to water molecules in an aqueous solution (0–6), *HBA* estimated number of hydrogen bonds that would be accepted by the solute from water molecules in an aqueous solution (2–20), *Ruleof5* number of violations of Lipinski's rule of five (max 4), *Ruleof3* number of violations of Jorgensen's rule of three (max 3), *CNS* predicted central nervous system activity on a −2 (inactive) to +2 (active) scale, *LogP* predicted octanol/water partition coefficient (−2.0–6.5), *LogHERG* predicted IC_{50} value for blockage of HERG K^+ channels (concern below −5), *PCaco* predicted apparent Caco-2 cell permeability in nm/s. (<25 poor, >500 great), *LogBB* predicted brain/blood partition coefficient (−3.0–1.2), *PMDCK* predicted apparent MDCK cell permeability in nm/sec. (<25 poor, >500 great), *LogKhsa* prediction of binding to human serum albumin (−1.5–1.5), *HOA%* predicted human oral absorption on 0 to 100% scale (>80% is high, <25% is poor)

morpholino-3(2*H*)-pyridazinone-2-arylpiperazinylacetamide showing good predicted druglikeness property and ADME profile, serves as a new scaffold for SIRT2 inhibition and pharmacophore identification of these compounds may provide a foundation for further exploration in this field.

Experimental

Molecular docking

The molecular docking studies were carried out using Glide implemented in the Schrödinger Small-Molecule Drug Discovery Suite (Small-Molecule Drug Discovery Suite 2020-2, Schrödinger, LLC, New York, NY, 2020). The compounds which were built via builder panel in Maestro were subjected to ligand preparation by LigPrep (Schrödinger Release 2020-2: LigPrep, Schrödinger, LLC, New York, NY, 2020) using default conditions. The x-ray crystal structure of SIRT2 (PDB: 5DY4) [44] was retrieved from the Protein Data Bank. The protein was prepared using the Protein Preparation Wizard tool. Water molecules except HOH549 were deleted and hydrogen atoms were added followed by assignment of all atom charges and atom types. Finally, energy minimization and refinement of the structures were done up to 0.3 Å RMSD by applying OPLS3e force field. Centroid of the X-ray ligand was defined as the grid box at coordinates X: −17.48; Y: −27.77; Z: 13.2. Van der Waals (vdW) radius scaling factor 1.00, partial charge cutoff 0.25, and OPLS3e force filed were used for receptor grid generation. The compounds prepared by LigPrep were docked into SIRT2 using the extra-precision (XP) docking mode of the Glide without any constraints and a 0.80 vdW radius scaling factor and 0.15 partial charge cutoff [47]. The protocol facilitates docking by ligand flexibility and generation of multiple conformers within the rigid receptor. The output poses were rescored by postprocess with Prime MM-GBSA calculation to obtain ligand binding energies. The compounds which are docked most favorably were ranked based on XP Gscore.

In vitro SIRT2 inhibition assay

The SIRT2 inhibition assay was performed using Fluor de Lys SIRT2 Fluorometric Drug Discovery Kits (BML-

AK556-0001, Enzo Life Sciences), according to the supplier's protocol. Briefly, test compounds in 1% (v/v) final DMSO concentration and/or SIRT assay buffer (10 µl/well) and human recombinant SIRT2 enzyme (BML-SE25) were incubated at 37 °C for 1 h. Then, NAD^+ and Fluor de Lys deacetylase substrate (25 µl/well, BML-KI179) were added to the mixture. The reaction mixture was incubated at 37 °C for 1 h. After that, the reaction was stopped by adding Fluor de Lys Developer II (BML-KI176) and nicotinamide 2 mM in SIRT assay buffer (total volume 50 µl), and the incubation was continued for 45 min at 37 °C. Fluorescence readings were obtained using a fluorometric plate reader with excitation wavelength 360 nm and emission 460 nm. The value of inhibition% was calculated from the fluorescence readings of inhibited wells relative to those of control wells.

Acknowledgements We are grateful to Prof. Mustafa Fethi SAHIN (Eastern Mediterranean University, Faculty of Pharmacy) for his supervisor's contributions in design and synthesis of the in-house compounds.

Compliance with ethical standards

Conflict of interest The authors declare no competing interests.

Publisher's note Springer Nature remains neutral with regard to jurisdictional claims in published maps and institutional affiliations.

References

1. Du J, Jiang H, Lin H. Investigating the ADP-ribosyltransferase activity of Sirtuins with NAD Analogues and ^{32}P-NAD. Biochemistry. 2009;48:2878–90. https://doi.org/10.1021/bi802093g.
2. Jiang H, Khan S, Wang Y, Charron G, He B, Sebastian C, et al. SIRT6 regulates TNF-α secretion through hydrolysis of long-chain fatty acyl lysine. Nature. 2013;496:110–3. https://doi.org/10.1038/nature12038.
3. Du J, Zhou Y, Su X, Yu JJ, Khan S, Jiang H, et al. Sirt5 is a NAD-dependent protein lysine demalonylase and desuccinylase. Science 2011;334:806. https://doi.org/10.1126/science.1207861.
4. Sauve AA, Wolberger C, Schramm VL, Boeke JD. The biochemistry of sirtuins. Annu Rev Biochem 2006;75:435–65. https://doi.org/10.1146/annurev.biochem.74.082803.133500.
5. North BJ, Marshall BL, Borra MT, Denu JM, Verdin E. The Human Sir2 Ortholog, SIRT2, is an NAD^+-dependent tubulin deacetylase. Mol Cell. 2003;11:437–44. https://doi.org/10.1016/S1097-2765(03)00038-8.
6. Zhang L, Kim S, Ren X. The clinical significance of SIRT2 in malignancies: a tumor suppressor or an oncogene? Front Oncol. 2020;10:1721. https://doi.org/10.3389/fonc.2020.01721.
7. Zhao Y, Wang L, Yang J, Zhang P, Ma K, Zhou J, et al. Anti-neoplastic activity of the cytosolic FoxO1 results from autophagic cell death. Autophagy. 2010;6:988–90. https://doi.org/10.4161/auto.6.7.13289.
8. Xu Y, Li F, Lv L, Li T, Zhou X, Deng C-X, et al. Oxidative stress activates SIRT2 to deacetylate and stimulate phosphoglycerate mutase. Cancer Res. 2014;74:3630. https://doi.org/10.1158/0008-5472.CAN-13-3615.
9. Zhang H, Park S-H, Pantazides BG, Karpiuk O, Warren MD, Hardy CW, et al. SIRT2 directs the replication stress response through CDK9 deacetylation. Proc Natl Acad Sci USA. 2013;110:13546. https://doi.org/10.1073/pnas.1301463110.
10. Beirowski B, Gustin J, Armour SM, Yamamoto H, Viader A, North BJ, et al. Sir-two-homolog 2 (Sirt2) modulates peripheral myelination through polarity protein Par-3/atypical protein kinase C (aPKC) signaling. Proc Natl Acad Sci USA. 2011;108:E952. https://doi.org/10.1073/pnas.1104969108.
11. Wang Y-P, Zhou L-S, Zhao Y-Z, Wang S-W, Chen L-L, Liu L-X, et al. Regulation of G6PD acetylation by SIRT2 and KAT9 modulates NADPH homeostasis and cell survival during oxidative stress. EMBO J. 2014;33:1304–20. https://doi.org/10.1002/embj.201387224.
12. Lagunas-Rangel FA. Current role of mammalian sirtuins in DNA repair. DNA Repair. 2019;80:85–92. https://doi.org/10.1016/j.dnarep.2019.06.009.
13. Ng F, Tang BL. Sirtuins' modulation of autophagy. J Cell Physiol. 2013;228:2262–70. https://doi.org/10.1002/jcp.24399.
14. Seung Min J, Haigis MC. Sirtuins in cancer: a balancing act between genome stability and metabolism. Mol Cells. 2015;38:750–8. https://doi.org/10.14348/molcells.2015.0167.
15. Carafa V, Rotili D, Forgione M, Cuomo F, Serretiello E, Hailu GS, et al. Sirtuin functions and modulation: from chemistry to the clinic. Clin Epigenetics. 2016;8:61. https://doi.org/10.1186/s13148-016-0224-3.
16. Zhang Y, Anoopkumar-Dukie S, Arora D, Davey AK. Review of the anti-inflammatory effect of SIRT1 and SIRT2 modulators on neurodegenerative diseases. Eur J Pharmacol. 2020;867:172847. https://doi.org/10.1016/j.ejphar.2019.172847.
17. Jing H, Hu J, He B, Negrón Abril YL, Stupinski J, Weiser K, et al. A SIRT2-selective inhibitor Promotes c-Myc oncoprotein degradation and exhibits broad anticancer activity. Cancer Cell. 2016;29:297–310. https://doi.org/10.1016/j.ccell.2016.02.007.
18. Shah AA, Ito A, Nakata A, Yoshida M. Identification of a selective SIRT2 inhibitor and its anti-breast cancer activity. Biol Pharm Bull. 2016;39:1739–42. https://doi.org/10.1248/bpb.b16-00520.
19. Moniot S, Forgione M, Lucidi A, Hailu GS, Nebbioso A, Carafa V, et al. Development of 1,2,4-oxadiazoles as potent and selective inhibitors of the human deacetylase sirtuin 2: structure–activity relationship, x-ray crystal structure, and anticancer activity. J Med Chem. 2017;60:2344–60. https://doi.org/10.1021/acs.jmedchem.6b01609.
20. Rumpf T, Schiedel M, Karaman B, Roessler C, North BJ, Lehotzky A, et al. Selective Sirt2 inhibition by ligand-induced rearrangement of the active site. Nat Commun. 2015;6:6263. https://doi.org/10.1038/ncomms7263.
21. Quinti L, Casale M, Moniot S, Pais Teresa F, Van Kanegan Michael J, Kaltenbach Linda S, et al. SIRT2- and NRF2-targeting thiazole-containing compound with therapeutic activity in huntington's disease models. Cell Chem Biol. 2016;23:849–61. https://doi.org/10.1016/j.chembiol.2016.05.015.
22. Outeiro TF, Kontopoulos E, Altmann SM, Kufareva I, Strathearn KE, Amore AM, et al. Sirtuin 2 inhibitors rescue α-Synuclein-mediated toxicity in models of parkinson's disease. Science. 2007;317:516–9. https://doi.org/10.1126/science.1143780.
23. Taylor DM, Balabadra U, Xiang Z, Woodman B, Meade S, Amore A, et al. A brain-permeable small molecule reduces neuronal cholesterol by inhibiting activity of sirtuin 2 deacetylase. ACS Chem Biol. 2011;6:540–6. https://doi.org/10.1021/cb100376q.
24. Ai T, Wilson DJ, More SS, Xie J, Chen L. 5-((3-Amidobenzyl) oxy)nicotinamides as sirtuin 2 inhibitors. J Med Chem. 2016;59:2928–41. https://doi.org/10.1021/acs.jmedchem.5b01376.
25. Seifert T, Malo M, Kokkola T, Engen K, Fridén-Saxin M, Wallén EAA, et al. Chroman-4-one- and chromone-based sirtuin 2 inhibitors with antiproliferative properties in cancer cells. J Med Chem. 2014;57:9870–88. https://doi.org/10.1021/jm500930h.

26. Wang L, Li C, Chen W, Song C, Zhang X, Yang F, et al. Discovery of (5-phenylfuran-2-yl)methanamine derivatives as new human sirtuin 2 inhibitors. Molecules. 2019;24:2724. https://doi.org/10.3390/molecules24152724.
27. Radwan MO, Ciftci HI, Ali TFS, Koga R, Tateishi H, Nakata A, et al. Structure activity study of S-trityl-cysteamine dimethylaminopyridine derivatives as SIRT2 inhibitors: Improvement of SIRT2 binding and inhibition. Bioorg Med Chem Lett. 2020;30:127458. https://doi.org/10.1016/j.bmcl.2020.127458.
28. Khalil NA, Ahmed EM, Zaher AF, El-Zoghbi MS, Sobh EA. Synthesis of certain benzothieno[3,2-d]pyrimidine derivatives as a selective SIRT2 inhibitors. Eur J Med Chem. 2020;187:111926. https://doi.org/10.1016/j.ejmech.2019.111926.
29. Eren G, Bruno A, Guntekin-Ergun S, Cetin-Atalay R, Ozgencil F, Ozkan Y, et al. Pharmacophore modeling and virtual screening studies to identify novel selective SIRT2 inhibitors. J Mol Graph Model. 2019;89:60–73. https://doi.org/10.1016/j.jmgm.2019.02.014.
30. Yagci S, Gozelle M, Kaya SG, Ozkan Y, Aksel AB, Bakar-Ates F, et al. Hit-to-lead optimization on aryloxybenzamide derivative virtual screening hit against SIRT. Bioorg Med Chem. 2021;30:115961. https://doi.org/10.1016/j.bmc.2020.115961.
31. Akhtar W, Shaquiquzzaman M, Akhter M, Verma G, Khan MF, Alam MM. The therapeutic journey of pyridazinone. Eur J Med Chem. 2016;123:256–81. https://doi.org/10.1016/j.ejmech.2016.07.061.
32. Süküroglu M, Küpeli E, Banoglu E, Ünlü S, Yesilada E, Sahin MF. Synthesis and analgesic activity of some 4,6-disubstituted-3(2h)-pyridazinone derivatives. Arzneimittelforschung. 2006;56:337–45. https://doi.org/10.1055/s-0031-1296731.
33. Ochiai K, Takita S, Eiraku T, Kojima A, Iwase K, Kishi T, et al. Phosphodiesterase inhibitors. Part 3: Design, synthesis and structure–activity relationships of dual PDE3/4-inhibitory fused bicyclic heteroaromatic-dihydropyridazinones with anti-inflammatory and bronchodilatory activity. Bioorg Med Chem. 2012;20:1644–58. https://doi.org/10.1016/j.bmc.2012.01.033.
34. Abouzid K, Bekhit SA. Novel anti-inflammatory agents based on pyridazinone scaffold; design, synthesis and in vivo activity. Bioorg Med Chem. 2008;16:5547–56. https://doi.org/10.1016/j.bmc.2008.04.007.
35. Sharma D, Bansal R. Synthesis of 2-substituted-4-aryl-6-phenylpyridazin-3(2H)-ones as potential anti-inflammatory and analgesic agents with cardioprotective and ulcerogenic sparing effects. Med Chem Res. 2016;25:1574–89. https://doi.org/10.1007/s00044-016-1588-9.
36. Asano T, Yamazaki H, Kasahara C, Kubota H, Kontani T, Harayama Y, et al. Identification, Synthesis, and biological evaluation of 6-[(6R)-2-(4-fluorophenyl)-6-(hydroxymethyl)-4,5,6,7-tetrahydropyrazolo[1,5-a]pyrimidin-3-yl]-2-(2-methylphenyl)pyridazin-3(2H)-one (AS1940477), a potent p38 MAP Kinase inhibitor. J Med Chem. 2012;55:7772–85. https://doi.org/10.1021/jm3008008.
37. Yue Q, Zhao Y, Hai L, Zhang T, Guo L, Wu Y. First synthesis of novel 3,3′-bipyridazine derivatives as new potent anti-hepatocellular carcinoma agents. Tetrahedron. 2015;71:7670–5. https://doi.org/10.1016/j.tet.2015.07.063.
38. Zhou S, Liao H, He C, Dou Y, Jiang M, Ren L, et al. Design, synthesis and structure–activity relationships of novel 4-phenoxyquinoline derivatives containing pyridazinone moiety as potential antitumor agents. Eur J Med Chem. 2014;83:581–93. https://doi.org/10.1016/j.ejmech.2014.06.068.
39. Csókás D, Zupkó I, Károlyi BI, Drahos L, Holczbauer T, Palló A, et al. Synthesis, spectroscopy, X-ray analysis and in vitro antiproliferative effect of ferrocenylmethylene-hydrazinylpyridazin-3(2H)-ones and related ferroceno[d]pyridazin-1(2H)-ones. J Organomet Chem. 2013;743:130–8. https://doi.org/10.1016/j.jorganchem.2013.06.040.
40. Al-Tel TH. Design and synthesis of novel tetrahydro-2H-pyrano[3,2-c]pyridazin-3(6H)-one derivatives as potential anticancer agents. Eur J Med Chem. 2010;45:5724–31. https://doi.org/10.1016/j.ejmech.2010.09.029.
41. Zimmerman G, Soreq H. Termination and beyond: acetylcholinesterase as a modulator of synaptic transmission. Cell Tissue Res. 2006;326:655–69. https://doi.org/10.1007/s00441-006-0239-8.
42. Lin H, Fang H, Wang J, Meng Q, Dai X, Wu S, et al. Discovery of a novel 2,3,11,11a-tetrahydro-1H-pyrazino[1,2-b]isoquinoline-1,4(6H)-dione series promoting neurogenesis of human neural progenitor cells. Bioorg Med Chem Lett. 2015;25:3748–53. https://doi.org/10.1016/j.bmcl.2015.05.084.
43. Boukharsa Y, Meddah B, Tiendrebeogo RY, Ibrahimi A, Taoufik J, Cherrah Y, et al. Synthesis and antidepressant activity of 5-(benzo[b]furan-2-ylmethyl)-6-methylpyridazin-3(2H)-one derivatives. Med Chem Res. 2016;25:494–500. https://doi.org/10.1007/s00044-015-1490-x.
44. Schiedel M, Rumpf T, Karaman B, Lehotzky A, Oláh J, Gerhardt S, et al. Aminothiazoles as potent and selective Sirt2 inhibitors: a structure–activity relationship study. J Med Chem. 2016;59:1599–612. https://doi.org/10.1021/acs.jmedchem.5b01517.
45. Fagbohun OF, Olawoye B, Ademakinwa AN, Oriyomi OV, Fagbohun OS, Fadare OA, et al. UHPLC/GC-TOF-MS metabolomics, MTT assay, and molecular docking studies reveal physostigmine as a new anticancer agent from the ethyl acetate and butanol fractions of *Kigelia africana* (Lam.) Benth. fruit extracts. Biomed Chromatogr. 2021;35:e4979. https://doi.org/10.1002/bmc.4979.
46. Fagbohun OF, Oriyomi OV, Adekola MB, Msagati TAM. Biochemical applications of *Kigelia africana* (Lam.) Benth. fruit extracts in diabetes mellitus. Comp Clin Path. 2020;29:1251–64. https://doi.org/10.1007/s00580-020-03179-9.
47. Friesner RA, Murphy RB, Repasky MP, Frye LL, Greenwood JR, Halgren TA, et al. Extra precision glide: Docking and scoring incorporating a model of hydrophobic enclosure for protein −ligand complexes. J Med Chem. 2006;49:6177–96. https://doi.org/10.1021/jm051256o.